

ADA 120789

12

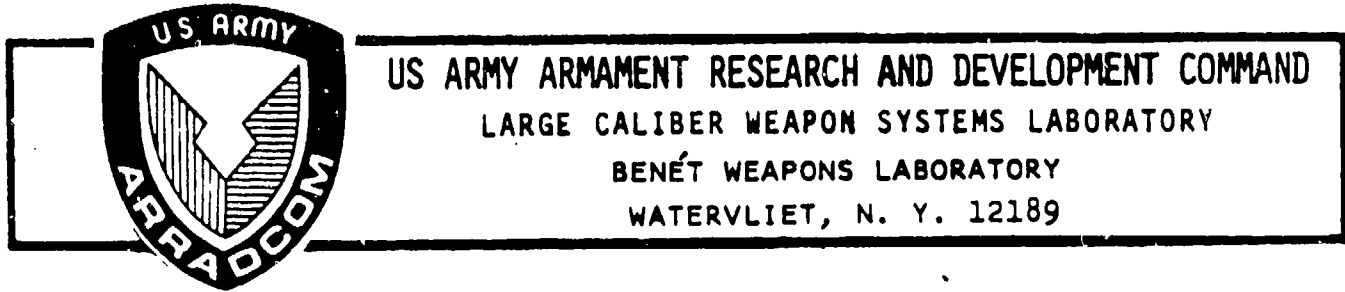
AD

TECHNICAL REPORT ARLCB-TR-82027

STRESS INTENSITY AND FATIGUE CRACK GROWTH IN A  
PRESSURIZED, AUTOFRETTAGED THICK CYLINDER

A. P. Parker  
J. H. Underwood  
J. F. Throop  
C. P. Andrasic

September 1982



AMCMS No. 6111.01.91A0.0

DA Project No. DT16110191A

PRON No. 1A1281501A1A

SEP 27 1982

APPROVED FOR PUBLIC RELEASE; DISTRIBUTION UNLIMITED

DTIC FILE COPY

#### DISCLAIMER

The findings in this report are not to be construed as an official Department of the Army position unless so designated by other authorized documents.

The use of trade name(s) and/or manufacture(s) does not constitute an official indorsement or approval.

#### DISPOSITION

Destroy this report when it is no longer needed. Do not return it to the originator.

REPORT DOCUMENTATION PAGE		READ INSTRUCTIONS BEFORE COMPLETING FORM
1. REPORT NUMBER ARLCB-TR-82027	2. GOVT ACCESSION NO. AD-A120 789	3. RECIPIENT'S CATALOG NUMBER
4. TITLE (and Subtitle) STRESS INTENSITY AND FATIGUE CRACK GROWTH IN A PRESSURIZED, AUTOFRETTAGED THICK CYLINDER		5. TYPE OF REPORT & PERIOD COVERED Final
		6. PERFORMING ORG. REPORT NUMBER
7. AUTHOR(s) A. P. Parker <sup>1</sup> J. F. Throop <sup>2</sup> J. H. Underwood <sup>2</sup> C. P. Andrasic <sup>3</sup>		8. CONTRACT OR GRANT NUMBER(s)
9. PERFORMING ORGANIZATION NAME AND ADDRESS US Army Armament Research & Development Command Benet Weapons Laboratory, DRDAR-LCB-TL Watervliet, NY 12189		10. PROGRAM ELEMENT, PROJECT, TASK AREA & WORK UNIT NUMBERS AMCMS No. 6111, 01.91A0.0 DA Project No. 1T16110191A PRON No. 1A1281501A1A A
11. CONTROLLING OFFICE NAME AND ADDRESS US Army Armament Research & Development Command Large Caliber Weapon Systems Laboratory Dover, NJ 07801		12. REPORT DATE September 1982
		13. NUMBER OF PAGES 45
14. MONITORING AGENCY NAME & ADDRESS (if different from Controlling Office)		15. SECURITY CLASS. (of this report) UNCLASSIFIED
		15a. DECLASSIFICATION/DOWNGRADING SCHEDULE
16. DISTRIBUTION STATEMENT (of this Report)  Approved for public release; distribution unlimited.		
17. DISTRIBUTION STATEMENT (of the abstract entered in Block 20, if different from Report)		
18. SUPPLEMENTARY NOTES  Presented at Fourteenth National Symposium on Fracture Mechanics, UCLA, Los Angeles, CA, 29 June - 1 July 1981. Published in ASTM Special Technical Publication.		
19. KEY WORDS (Continue on reverse side if necessary and identify by block number) Crack Growth                      Fracture (Materials) Fatigue Crack                      Residual Stress Cylinders                              Stress Intensity Factor		
20. ABSTRACT (Continue on reverse side if necessary and identify by block number) Stress intensity factors are determined, using the modified mapping collocation (MMC) method for a single, radial, straight-fronted crack in a thick cylindrical tube which has been subjected to full autofrettage treatment (100 percent over-strain). By superposition of these results and existing solutions, stress intensity factors are determined for the same geometry with internal pressure and any amount of overstrain from zero to 100 percent. (CONT'D ON REVERSE)		

## 7. AUTHOR(S) (CONT'D):

<sup>1</sup>Guest Scientist, US Army Materials and Mechanics Research Center, Watertown, MA, from The Royal Military College of Science, Shrivenham, SN6 8LA, England.

<sup>2</sup>Research Engineers, USA ARRADCOM, Watervliet, NY.

<sup>3</sup>Research Scientist, The Royal Military College of Science, Shrivenham, SN6 8LA England.

## 20. ABSTRACT (CONT'D):

Correction factors for crack shape and non-ideal material yielding are determined from various sources for the pressurized, autofrettaged tubes containing semi-elliptical cracks. These results are employed in the life prediction of pressurized thick tubes with straight-fronted and semi-circular cracks, for various amounts of autofrettage. Experimentally determined lifetimes for tubes having zero and 30 percent nominal overstrain are significantly greater than the predictions for both straight fronted and semi-circular cracks. This is related to multiple initiation and early growth of cracks from the notch.

Experimentally determined lifetimes for a tube with a 60 percent nominal overstrain are somewhat less than predicted. This effect is partially explained by additional experimental work which shows that the angle of opening of rings cut from autofrettaged tubes is somewhat less than the ideal predictions. The latter effect is attributed to the Bauschinger effect and the associated reduced yield strength in compression during the unloading of tubes during the autofrettage process.



A

## TABLE OF CONTENTS

	<u>Page</u>
ACKNOWLEDGEMENTS	iii
NOMENCLATURE	iv
INTRODUCTION	1
CALCULATION OF STRESS INTENSITY FACTORS	2
Loading A	5
Loading B	6
Loading C	7
CORRECTION FOR THE CRACK SHAPE EFFECTS	8
EFFECTS OF NONIDEAL RESIDUAL STRESS DISTRIBUTION	14
LIFE CALCULATIONS	17
DISCUSSION AND CONCLUSIONS	21
REFERENCES	24
APPENDIX	A-1
APPENDIX REFERENCES	A-4

### TABLES

I. COMPARISON OF K VALUES FOR DEEPLY CRACKED CYLINDER AND PLATE	12
-----------------------------------------------------------------	----

### LIST OF ILLUSTRATIONS

1. Cracked thick cylinder geometry showing partitioning and mapping schemes. (a) z (physical) plane, (b) $\xi$ plane, (c) $\zeta$ plane.	27
2. Stress intensity factors for a single, straight-fronted, radial crack in a thick cylinder. (Inset) Short crack length convergence for 100 percent overstrain.	28
3. Stress intensity factors for a single, straight-fronted crack in a pressurized thick cylinder with 0 percent, 30 percent, 60 percent and 100 percent overstrain.	29

	<u>Page</u>
4. Semi-elliptical crack in a thick cylinder.	30
5. (a) Crack shape factors for a plate in tension ( $\phi = \pi/2$ ), after Reference 14.	31
(b) Crack shape factors for a plate in pure bending ( $\phi = \pi/2$ ), after Reference 14.	
6. (a) Method of calculating proportion of tension and bending, pressure in bore and cracks.	32
(b) Crack shape factors for pressure in bore and cracks, $a/c = 0.8$ , $\phi = \pi/2$ .	
(c) Crack shape factors for pressure in bore and cracks, $a/c = 0.8$ , $\phi = 0$ .	
7. (a) Crack shape factors, $L_p$ , for pressure in bore and cracks, $\phi = \pi/2$ ; two data points from Reference 14, $a/c = 1.0$ .	33
(b) Crack shape factors, $L_p$ , for pressure in bore and cracks, $\phi = 0$ ; two data points from Reference 14, $a/c = 1.0$ .	
(c) Crack shape factors, $L_a$ , for 100 percent overstrain, $\phi = \pi/2$ .	
(d) Crack shape factors, $L_a$ , for 100 percent overstrain, $\phi = 0$ .	
8. Ratio of opening angle for partial overstrain to the theoretical value for 100 percent overstrain.	34
9. Fatigue crack growth (a versus N) in thick cylinder with single, straight-fronted crack; experimental results and predictions.	35
10. Fatigue crack growth (a versus N) in thick cylinder with single, semi-circular crack; experimental results and predictions.	36

#### ACKNOWLEDGMENTS

The first author performed work on this paper during a TTCP attachment to the Engineering Mechanics Laboratory, US Army Materials and Mechanics Research Center. The fourth author acknowledges support from a UK Ministry of Defense research contract as a Research Scientist at the Royal Military College of Science.

## NOMENCLATURE

a	Crack depth
A	Autofrettage
c	Surface crack length
C	Coefficient in Paris' crack growth law
E	Modulus of elasticity
G	$E/2(1+\nu)$
H <sub>C</sub>	Correction factor defined in equation (11)
K	Stress intensity factor
K <sub>I</sub>	Opening mode stress intensity factor
K <sub>II</sub>	Sliding mode stress intensity factor
$\tilde{K}$	Non-dimensionalizing stress intensity factor
K <sub>0</sub>	Non-dimensionalizing stress intensity factor
$\Delta K$	Stress intensity factor range
ln	Natural logarithm
m	Exponent in Paris' crack growth law
max	Maximum
min	Minimum
N	Number of loading cycles
p	Pressure
PB	Pure bending
PT	Pure tension
r	Radius
R <sub>1</sub>	Tube inner radius

$R_2$	Tube outer radius
$R_A$	Tube autofrettage radius
$R_D$	Tube reversed yielding radius
$t$	Theoretical
$Y$	Yield stress
$z$	Complex variable, $x + iy$
$\alpha$	Proportion of tension
$\beta$	Proportion of bending
$\gamma$	Tube opening angle (radians)
$\zeta$	Parameter plane
$\theta$	Angular coordinate
$\kappa$	$3-4\nu$ (plane strain), $(3-\nu)/(1+\nu)$ (plane stress)
$\lambda$	Yield stress in tension/yield stress in compression
$\nu$	Poisson's ratio
$\xi$	Parameter plane
$\sigma$	Direct stress
$\tau$	Shear stress
$\phi$	Complex stress function
$\psi$	Complex stress function

## INTRODUCTION

Fatigue crack growth arising from the cyclic pressurization of thick-wall cylinders tends to produce radial fatigue cracks emanating from the bore. A knowledge of the crack tip stress intensity factor,  $K$ , is necessary in order to predict the fatigue crack growth rate, critical length and lifetime of such cracks. It is common practice to produce an advantageous stress distribution by autofrettage (overstrain) of the cylinder in order to slow or prevent crack growth. This autofrettage process may involve plastic strain throughout the wall thickness, or any lesser proportion of the wall thickness, depending upon the degree of overstrain applied to the cylinder by over pressure or by an oversized mandrel-swage process.

An accurate stress intensity solution for pressurized, autofrettaged thick cylinders is a fundamental requirement for crack growth rate and life prediction. Some of the work relating to two and three dimensional  $K$  solutions is reviewed by Tan and Fenner.<sup>1</sup> Of the various types of solutions, the errors associated with collocation and integral equation solutions are of the order of 1 percent, while 4 percent would be more typical of finite element and boundary element methods. However, there may be more significant uncertainties in crack growth and life prediction. Some key factors, and the factors considered here, are the shape of the crack during the fatigue lifetime of the component, uncertainty over the exact proportion of overstrain in the tube, and a residual stress distribution which generally does not conform with

---

<sup>1</sup>Tan, C. L. and Fenner, R. T., "Stress Intensity Factors for Semi-Elliptical Surface Cracks in the Pressurized Cylinders Using the Boundary Integral Equation Method," Int. J. Fracture, Vol. 16, No. 3, 1980, pp. 233-245.

the predictions of an idealized elastic-plastic analysis, particularly the assumption of the same magnitude of yield strength in tension and compression.

In this report it is proposed that accurate two dimensional K solutions may be modified in order to predict stress intensity factors, and hence crack growth rates, for semi-elliptical cracks in pressurized thick-wall cylinders with residual stress distributions. Such predictions may be compared with experimental crack growth data, and some measure of the extent of overstrain may be obtained by cutting autofrettaged tubes radially, and measuring the angle of opening.

#### CALCULATION OF STRESS INTENSITY FACTORS

Stress intensity factors for the plane (two dimensional) geometry illustrated in Figure 1(a) were obtained by the modified mapping collocation (MMC) method. This method is described in detail in Reference 2. Briefly, complex variable methods, due to Muskhelishvili<sup>3</sup> are utilized. Stresses and displacements within a body are given in terms of the complex stress functions  $\phi(z)$  and  $\psi(z)$  by:

$$\sigma_x + \sigma_y = 4 \operatorname{Re} \{ \phi'(z) \} \quad (1)$$

$$\sigma_y - \sigma_x + 2i \tau_{xy} = 2[ z \overline{\phi''(z)} + \psi'(z) ] \quad (2)$$

---

<sup>2</sup>Andrasic, C. P. and Parker, A. P., "Weight Functions for Cracked Curved Beams," Numerical Methods in Fracture Mechanics, D. R. J. Owen and A. R. Luxmoore (Eds.), Proceedings Second International Conference, Swansea, 1980, pp. 67-82.

<sup>3</sup>Muskhelishvili, N. I., Some Basic Problems of the Mathematical Theory of Elasticity, Noordhoff, 1973.

$$2G(u+iv) = \kappa \phi(z) - z\overline{\phi'(z)} - \overline{\psi(z)} \quad (3)$$

where the complex variable  $z = x + iy$ ,  $x$  and  $y$  are the physical coordinates, primes denote differentiation, and bars represent the complex conjugate.

Also:

$$G = \frac{E}{2(1+\nu)}$$

$$\kappa = 3 - 4\nu \text{ (plane strain), } \kappa = \frac{3-\nu}{1+\nu} \text{ (plane stress)}$$

where  $G$  is the shear modulus,  $E$  the elastic modulus, and  $\nu$  is Poisson's ratio, while the resultant force over an arc  $s$  is:

$$f_1 + if_2 = i \int_s (X_n + iY_n) ds = \phi(z) + z\overline{\phi'(z)} + \overline{\psi(z)} \quad (4)$$

where  $X_n ds$  and  $Y_n ds$  are the horizontal and vertical components of force acting on  $ds$ .

The solution of the cracked, autofrettaged cylinder was carried out on similar lines to that of Tracy.<sup>4</sup> A complex mapping transforms straight lines parallel to the real axis in the  $\xi$ -plane to curved lines in the physical ( $z$ ) plane, in particular the real axis in the  $\xi$  plane is mapped to an arc of radius  $R_1$ , centered at the origin in the  $z$ -plane, Figure 1. A further mapping is introduced which maps the unit semi-circle plus its exterior in the  $\zeta$  plane to the crack plus its exterior in the  $\xi$ -plane, see Figure 1(b,c). The analytic continuation arguments of Muskhelishvili<sup>1</sup> are used to ensure traction-

---

<sup>4</sup>Tracy, P. G., "Elastic Analysis of Radial Cracks Emanating From the Outer and Inner Surfaces of a Circular Ring," Engng. Frac. Mech., Vol. 11, 1979, pp. 291-300.

free conditions along F'L' and J'G' and hence FL and JG in the physical plane, Figure 1.

For certain geometries it is necessary to use partitioning<sup>2</sup> to obtain the desired accuracy. The partitioning of the cylinder is shown in Figure 1. In general each region has its own complex stress and mapping function. Since there is symmetry about the imaginary axis, only region I and that part of region II to the right of the imaginary axis need be considered. When partitioning is used it is necessary to "stitch" along common boundaries, by imposing equilibrium and compatibility of displacements.

In the MMC method the infinite series representations of the stress functions are truncated to a finite number of terms. Force conditions are imposed at selected boundary points which give conditions on the unknown coefficients in the stress functions. Thus each boundary point produces two rows in the main matrix A, and two corresponding elements in the boundary conditions vector  $b$ , where:

$$A x = b$$

and  $x$  is the vector of unknown coefficients. The common ("stitched") boundary points are used to obtain conditions relating the unknown coefficients. Each common boundary point gives four rows in A and four corresponding zeros in  $b$ . In general, A is a matrix of  $l$  rows and  $m$  columns, where  $l$  and  $m$  depend upon the number of boundary points and unknown coefficients respectively. It was found that convergence is generally better when  $2m < l < 2.5 m$ , and this

---

<sup>2</sup>Andrasic, C. P. and Parker, A. P., "Weight Functions For Cracked Curved Beams," Numerical Methods in Fracture Mechanics, D. R. J. Owen and A. R. Luxmoore (Eds.), Proceedings Second International Conference, Swansea, 1980, pp. 67-82.

compares well with other workers.<sup>5</sup> A least-square error minimization procedure was used to solve the overdetermined set of linear equations. Knowing the coefficients for the stress function in the cracked region, the crack tip stress intensity factor,  $K$ , may be determined from:<sup>6</sup>

$$K = K_I - iK_{II} = 2(2\pi)^{1/2} \lim_{z \rightarrow z_c} (z-z_c)^{1/2} \cdot \phi'(z) \quad (5)$$

where  $K_I$  and  $K_{II}$  are opening and sliding mode stress intensity factors respectively, and  $z_c$  is the location of the crack tip.

We now consider the various loadings, and combinations of loadings which will be necessary for the solution of the pressurized, autofrettaged tube.

Loading A: Internal pressure acting in bore and cracks.

An accurate MMC opening mode stress intensity solution,  $K_I$ , is available for this configuration<sup>7</sup> and is shown as the upper curve in Figure 2. This MMC solution was obtained by superposition of an all-round tension field on the outer boundary. The results are presented in dimensionless form as  $K_I/K_p$ , where:

$$K_p = \frac{2R_2^2}{(R_2^2 - R_1^2)} p(\pi a)^{1/2} \quad (6)$$

and  $R_2$  is the outer radius,  $R_1$  the inner radius,  $a$  is the crack depth and  $p$  is the internal pressure acting in both bore and crack. Also shown, for the

<sup>5</sup>Fason, E. D., "A Review of Least Squares Methods for Solving Partial Differential Equations," Int. J. Num. Meth. in Engng., Vol. 10, 1976, pp. 1021-1046.

<sup>6</sup>Sih, G. C., Paris, P. C., and Erdogan, F., "Crack Tip Stress Intensity Factors for Plane Extension and Plate Bending Problems," J. Appl. Mech., Vol. 29, 1962, pp. 306-312.

<sup>7</sup>Bowie, O. L. and Freese, C. E., "Elastic Analysis For a Radial Crack in a Circular Ring," Engineering Fracture Mechanics, Vol. 4, No. 2, 1972, pp. 315-321.

purposes of comparison, are points from a solution due to Grandt<sup>8</sup> based on an approximate weight function method which was also employed in the derivation of additional solutions referred to in the next section.

Loading B: Ideal autofrettage residual stresses in uncracked tube.

An MMC program, based on the formulation outlined in this section, was used to calculate the stress intensity results for full autofrettage (100 percent overstrain), shown as the lower curve in Figure 2. This was based on the ideal, elastic-plastic solution,<sup>9</sup> where the distribution of hoop stress ( $\sigma_\theta$ ) in the uncracked tube is given by:

$$\sigma_\theta = -Y \ln (R_2/R_1) \left[ 1 + \frac{R_1^2}{R_2^2 - R_1^2} \left( 1 + \frac{R_2^2}{r^2} \right) \right] + Y [1 + \ln (r/R_1)] \quad (7)$$

and Y is the uniaxial yield strength of the material (Tresca's criterion) or 1.15 x yield strength (von 'ses' criterion). Points obtained from a solution by Grandt are shown for comparison purposes. The approximate results of Grandt<sup>10</sup> for a cracked tube of the same dimensions subjected to steady-state thermal loading were modified in accordance with Reference 11 to make possible a comparison with the calculated autofrettage results. The modification is based on the fact that the residual stress distribution for 100 percent over-

---

<sup>8</sup>Grandt, A. F., "Stress Intensity Factors For Cracked Holes and Rings Loaded With Polynomial Crack Face Pressure Distributions," Int. J. Fracture, Vol. 14, 1978, pp. R221-R229.

<sup>9</sup>Hill, R., The Mathematical Theory of Plasticity, Clarendon Press, Oxford, 1950.

<sup>10</sup>Grandt, A. F., "Two Dimensional Stress Intensity Factor Solutions For Radially Cracked Rings," AFML-TR-75-121, Air Force Materials Lab, Wright Patterson AFB, Ohio, 1975.

<sup>11</sup>Parker, A. P. and Farrow, J. R., "Stress Intensity Factors for Multiple Radial Cracks Emanating Form the Bore of an Autofrettaged or Thermally Stressed Thick Cylinder," Engng. Frac. Mech., Vol. 14, 1981, pp. 237-241.

strain is identical to that for steady state thermal loading, apart from a simple multiplying constant. Agreement is generally within 5 percent.

A particularly important feature of the MMC formulation outlined at the beginning of this section is the accuracy of the results at shallow crack depths. Many available results are not quoted for  $a/(R_2-R_1) < 0.1$ , or even 0.2, and are therefore of limited use for life prediction purposes. The inset in Figure 2 shows the calculated results for 100 percent overstrain in the range  $0 < a/(R_2-R_1) < 0.1$ , and indicates good convergence to the limiting value of 1.12. Since as much as 80 percent of gun tube lifetime may be expended in this range it is clearly very important to seek accurate results at shallow crack depths. It is apparent that this solution provides the required accuracy. The results for full autofrettage are presented in dimensionless form as  $K_I/K_A$  where:

$$K_A = [1 - 2n (R_2/R_1) \left( \frac{2R_2^2}{R_2^2 - R_1^2} \right)] Y (\pi a)^{1/2} \quad (8)$$

Loading C: Internal pressure and ideal autofrettage.

The total stress intensity in a pressurized, fully autofrettaged (100 percent overstrain) tube is given by the superposition of the results in Figure 2, thus:

$$K_{\text{Full autofrettage + pressure}} = K_p + K_A \quad (9)$$

where  $K_p$  is the stress intensity with pressure in bore and crack, and  $K_A$  is the stress intensity contribution due to the 100 percent overstrain residual stress field acting alone.

In the event that the tube has been subjected to less than 100 percent overstrain, the plastic flow during the autofrettage process will extend to a radius  $R_A$ , and the stress intensity factor in this case is given by:<sup>12</sup>

$$K_{\text{partial autofrettage}} + \text{pressure} = \left[ 1 + \frac{Y}{p} \ln(R_2/R_A) - \frac{Y}{p} (R_2^2 - R_A^2)/2R_2^2 \right] K_p + K_A, \\ a < R_A - R_1 \quad (10)$$

where  $R_A$  can be obtained from the expression:<sup>12</sup>

$$p = Y \ln(R_A/R_1) + \frac{Y}{2R_2^2} (R_2^2 - R_A^2)$$

Results for 0, 30, 60, and 100 percent overstrain, with  $Y/p = 3.55$ ,  $R_2/R_1 = 2.0$ , based on the superposition of results given in Figure 2 are shown in Figure 3. These curves indicate the very significant reduction in stress intensity as a result of the ideal autofrettage process. Indeed, for the particular value  $Y/p = 3.55$ , 100 percent overstrain causes a negative total stress intensity (i.e., crack closure) for crack depths up to  $a/(R_2 - R_1) = 0.08$ .

#### CORRECTION FOR THE CRACK SHAPE EFFECTS

Thus far we have ignored the effect of crack shape on stress intensity, assuming a through crack. We now consider the crack to be semi-elliptical, semi-major axis  $c$ , depth  $a$ , Figure 4. In order to modify the two-dimensional results to account for crack shape we employ two sets of work, namely the extensive results for semi-elliptical cracks in a flat plate under tension or

---

<sup>12</sup>Parker, A. P. and Farrow, J. R., "Stress Intensity Factors for Multiple Radial Cracks Emanating From the Bore of an Autofrettaged or Thermally Stressed Thick Cylinder," Engng. Frac. Mech., Vol. 14, 1981, pp. 237-241.

bending, due to Newman and Raju,<sup>13</sup> and the limited results for a semi-elliptical crack in a pressurized thick cylinder, due to Tan and Fenner<sup>1</sup> and Atluri and Kathiresan.<sup>14</sup>

First, consider the flat plate containing a semi-elliptical crack. From the results given in Reference 13, we may define a correction factor for the plate in pure tension  $H_{PT}$  given by:

$$H_{PT} = \frac{K_{PT}}{K_{PT}}$$

where  $K_{PT}$  is the stress intensity factor for semi-elliptical crack in a plate in tension and  $K_{PT}$  is the stress intensity factor solution for a straight-fronted through crack given in Reference 15. Curves of the correction factor  $H_{PT}$  are shown in Figure 5(a).

Similar correction factors for the flat plate under pure bending  $H_{PB}$  are defined by:

$$H_{PB} = \frac{K_{PB}}{K_{PB}}$$

where  $K_{PB}$  is the stress intensity factor for a semi-elliptical crack in a plate in pure bending and  $K_{PB}$  is the solution for a straight-fronted through crack.<sup>15</sup> Curves of the correction factor  $H_{PB}$  are shown in Figure 5(b).

---

<sup>1</sup>Tan, C. L. and Fenner, R. T., "Stress Intensity Factors for Semi-Elliptical Surface Cracks in Pressurized Cylinders Using the Boundary Integral Equation Method," Int. J. Fracture, Vol. 16, No. 3, 1980, pp. 233-245.

<sup>13</sup>Newman, J. C. and Raju, I. S., "Analyses of Surface Cracks in Finite Plates Under Tension or Bending Loads," NASA TP 1578, 1979.

<sup>14</sup>Atluri, N. and Kathiresan, K., "3D Analyses of Surface Flaws in Thick-Walled Reactor Pressure-Vessels Using Displacement-Hybrid Finite Element Method," Nuclear Engng. and Design, Vol. 51, 1979, pp. 163-176.

<sup>15</sup>Rooke, D. P. and Cartwright, D. J., Compendium of Stress Intensity Factors, Her Majesty's Stationery Office, London, 1976.

It is proposed that, at shallow crack depths, the correction factors applicable to the thick cylinder may be obtained by appropriate superpositions of  $H_{pT}$  and  $H_{pB}$ , given by,

$$H_C = \alpha H_{pT} + \beta H_{pB} \quad (11)$$

where the multiplying factors  $\alpha$  and  $\beta$  are obtained by calculating the proportions of tension and bending in the uncracked tube which act over the prospective crack line. In order to test this hypothesis, consider the case of a tube subjected to internal pressure. In this case the crack-line loading comprises hoop stresses due to the internal pressure<sup>12</sup> plus a contribution from the pressure,  $p$ , which infiltrates the crack, thus the total crack line loading is:

$$\sigma_{\theta} = p \left[ 1 + \frac{R_1^2}{R_2^2 - R_1^2} \left( 1 + \frac{R_2^2}{r^2} \right) \right]$$

as shown in Figure 6(a). Using a straight line approximation, for the range  $0 < a/(R_2 - R_1) < 0.2$ , the proportion of tension loading is given by  $\alpha = 1.72/2.66$  while the proportion of pure bending,  $\beta = 0.94/2.66$ , hence the correction factor  $H_C$  is determined as

$$H_C = .645 H_{pT} + .355 H_{pB}$$

Correction factors determined on this basis are plotted in Figure 6(b) for the case  $a/c = 0.8$ . Also shown are the equivalent correction factors obtained for the same configuration by Tan and Fenner,<sup>1</sup> using boundary

<sup>1</sup>Tan, C. L. and Fenner, R. T., "Stress Intensity Factors for Semi-Elliptical Surface Cracks in Pressurized Cylinders Using the Boundary Integral Equation Method," Int. J. Fracture, Vol. 16, No. 3, 1980, pp. 233-245.

<sup>12</sup>Parker, A. P., "Stress Intensity and Fatigue Crack Growth in Multiply-Cracked, Pressurized, Partially Autofrettaged Thick Cylinders," Fatigue of Engng. Materials and Structures (in press).

element methods. Agreement is within 2 percent at  $a/(R_2-R_1) = 0.2$ . For deeper cracks the difference between plate and cylinder results becomes appreciable because of the differences in constraint, discussed in the upcoming paragraph. It is important to emphasize that the proportion of the tube in which the vast majority of component lifetime is expended is well represented by the model, i.e., for  $a/(R_2-R_1) < 0.3$ . The equivalent correction factors for  $K$  at the point  $\phi = 0$  (the free surface of the plate) are shown in Figure 6(c) and exhibit similar characteristics to those of Figure 6(b).

The significant difference between the cylinder and plate shape factors in Figure 6(b) is attributed to the significantly greater constraint of a cylinder compared with a plate, particularly for straight-fronted, deep cracks. This difference can be demonstrated by comparing the  $K$  for a straight-fronted,  $a/(R_2-R_1) = 0.8$  crack in a pressurized cylinder with  $R_2/R_1 = 2.0$  with the  $K$  for a straight-fronted,  $a/(R_2-R_1) = 0.8$  crack in a plate with approximately the same combination of tension and bending loading as that of the pressurized cylinder. The  $K$  for the cylinder can be obtained from Reference 7 or from Figure 2 and is shown in Table I. The  $K$  for the plate with cylinder loading is obtained using the expressions for pure tension and pure bending<sup>15</sup> as follows:

$$K_{\text{plate}} = K_{\text{PT}} + K_{\text{PB}}$$

---

<sup>7</sup>Bowie, O. L. and Freese, G. E., "Elastic Analysis For a Radial Crack in a Circular Ring," Engineering Fracture Mechanics, Vol. 4, No. 2, 1972, pp. 315-321.

<sup>15</sup>Rooke, D. P. and Cartwright, D. J., Compendium of Stress Intensity Factors, Her Majesty's Stationery Office, London, 1976.

The tension and bending stresses in  $K_{PT}$  and  $K_{PB}$  are determined as  $\sigma_{PT} = 2.0 p$  and  $\sigma_{PB} = 0.5 p$ , by using a linear approximation of the entire cylinder loading plot shown in Figure 6(a). The  $K$  for the plate with a straight crack is several times that of the cylinder, which indicates that the plate is much less constrained. Therefore, the increase in constraint corresponding to a semi-elliptical rather than a straight crack will be much larger for a plate than for a cylinder. This results in the much smaller  $H_c$  for a plate than for a cylinder, as observed in Figure 6(b). When the final comparison is made in Table I,  $K$  for deep semi-elliptical cracks in a cylinder and a similarly loaded plate are about the same, as might be expected.

TABLE I. COMPARISON OF  $K$  VALUES FOR DEEPLY CRACKED CYLINDER AND PLATE

	$K$ for $a/(R_2-R_1) = 0.8$ straight crack	$H_c$ from Fig. 6(b) for $a/(R_2-R_1) = 0.8$ , $a/c = 0.8$	$K$ for $a/(R_2-R_1) = 0.8$ , $a/c = 0.8$ semi-elliptical crack
pressurized cylinder	$6.99 p(a)^{1/2}$	0.42	$2.9 p(a)^{1/2}$
plate with approx. cylinder loading	$46.7 p(a)^{1/2}$	0.07	$3.3 p(a)^{1/2}$

In order to obtain a range of correction factors applicable to thick cylinders, the procedure outlined by Eq. (11), Figure 6, and related discussion was used to obtain correction factors from Newman's work for the case of internal pressure, and full autofrettage (100 percent overstrain). These results for relatively short cracks were combined, using engineering

judgment, with those of Tan and Fenner for longer cracks to obtain correction factors for use over a wide range of crack length. The results for pressure,  $L_p$ , are shown in Figure 7(a) and 7(b), for  $\phi = \pi/2$  and 0.0 respectively, and for autofrettage,  $L_A$ , are shown in Figure 7(c) and 7(d) for  $\phi = \pi/2$  and 0.0 respectively. In the case of pressure, Figure 7(a) and 7(b), we may compare in each figure with the solutions due to Atluri and Kathiresan<sup>14</sup> at two points, namely  $a/c = 1.0$ ,  $a/t = 0.5$  and 0.8. For  $\phi = \pi/2$  agreement is within 8 percent, however, for  $\phi = 0$  the correction factors differ by 25 percent, reflecting wide disagreement between workers on K solutions at the free-surface.<sup>13,14</sup>

It is thus possible to calculate the stress intensity factor for any combination of pressure, ideal partial autofrettage and crack shape by correcting the stress intensity factors presented in Figure 2 in accordance with Eq. (10) and correction factors  $L_p$  and  $L_A$  to obtain:

$$\begin{aligned}
 K_{\text{partial autofrettage}} &= L_p \left[ 1 + \frac{Y}{P} \ln(R_2/R_A) - \frac{Y}{P} (R_2^2 - R_A^2)/2R_2^2 \right] K_p \\
 &+ \text{pressure (3D)} \\
 &+ L_A K_A
 \end{aligned} \tag{12}$$

<sup>13</sup>Newman, J. C. and Raju, I. S., "Analyses of Surface Cracks in Finite Plates Under Tension or Bending Loads," NASA TP 1578, 1979.

<sup>14</sup>Atluri, N. and Kathiresan, K., "3D Analyses of Surface Flaws in Thick-Walled Reactor Pressure-Vessels Using Displacement-Hybrid Finite Element Method," Nuclear Engng. and Design, Vol. 51, 1979, pp. 163-176.

## EFFECTS OF NONIDEAL RESIDUAL STRESS DISTRIBUTION

The residual stress distribution predicted by Eq. (7) may not occur in practice.<sup>16,17</sup> Non-ideal Bauschinger effects and uncertainty over the exact amount of autofrettage on unloading may produce a different stress distribution. In earlier work<sup>16</sup> a constant reduction factor of 0.7 was applied to the autofrettage contribution to stress intensity factor to account for primarily the Bauschinger effect.

In the present work it is proposed that these effects may be considered in a different manner. If an unflawed autofrettaged tube is cut along a radius, it will spring apart, the theoretical angle of opening  $\gamma_t$  being given for 100 percent overstrain and using the von Mises' yield criterion as:<sup>18</sup>

$$\gamma_t^{100\%} = \frac{8\pi Y}{\sqrt{3}E} \quad (13)$$

In the case of partial overstrain, the total moment acting over the cut ends is reduced by a factor  $F$ . Details of the calculation of  $F$  are contained in an Appendix. The theoretical angle of opening for partial overstrain  $\gamma_t^{\%}$  is given by:

$$\gamma_t^{\%} = F \gamma_t^{100\%} \quad (14)$$

---

<sup>16</sup>Underwood, J. H. and Throop, J. F., "Residual Stress Effects on Fatigue Cracking of Pressurized Cylinders and Notched Bending Specimens." presented at Fourth SESA International Congress, Boston, MA, May 1980.

<sup>17</sup>Milligan, R. V., Koo, W. H., Davidson, T. E., "The Bauschinger Effect in a High-Strength Steel," Trans. ASME, J. Bas. Engineering, Vol. 88, 1966, pp. 480-488.

<sup>18</sup>Parker, A. P. and Farrow, J. R., "On the Equivalence of Axisymmetric Bending, Thermal, and Autofrettage Residual Stress Fields," J. Strain Analysis, Vol. 15, No. 1, 1980, pp. 51-52.

A graphical representation of  $F$  for a tube having  $R_2/R_1 = 2.0$  is shown in Figure 8. The angle (and moment) ratio  $F$  between partial and 100 percent overstrain does not vary much with  $R_2/R_1$ . In fact, for tubes in the range  $1.8 < R_2/R_1 < 2.2$  the deviation from the curve in Figure 8 is only 1 percent, and of course it still goes asymptotically to the limit of 1.0 at 100 percent overstrain, and to zero at 0 percent overstrain.

We propose that a comparison of the ratio of measured opening angle to  $100\% \gamma_t$  with the ratio  $F$  provides an indication of the non-ideality of the residual stress distribution in actual autofrettage cylinders. The data points shown in Figure 8 make this comparison. Each point represents an autofrettaged steel cylinder of the type described in Reference 16. A section was removed from each cylinder, and the opening angle was measured using an optical comparator. The ratio of measured angle to 100 percent overstrain theoretical angle was calculated using the measured value of yield strength,  $Y$  for each tube.

The important features of the comparison between experiment and theory in Figure 8 are the following. (a) The experimental results are generally near or above the theoretical curve for relatively low overstrain and generally below the curve for high overstrain. This can be explained by the Bauschinger effect since, for high overstrain and the associated large amount of tensile yielding, the Bauschinger effect would result in significant reverse yielding and less than expected residual stress and opening angle. (b) The two sets of

---

<sup>16</sup>Underwood, J. H. and Throop, J. F., "Residual Stress Effects on Fatigue Cracking of Pressurized Cylinders and Notched Bending Specimens," presented at Fourth SESA International Congress, Boston, MA, May 1980.

experimental results designated by dashed lines indicate less than expected opening angle and residual stress with increasing  $R_2/R_1$ . This also is consistent with the Bauschinger effect, using a similar rationale as with (a), that is, larger  $R_2/R_1$  result in more tensile yielding, more reverse yielding, and less than expected residual stress.

Also shown in Figure 8 are the measured-to-theoretical angle ratios from the 30 percent and 60 percent overstrained tubes of the experimental work described here. Note that the average of the two angle measurements for 60 percent overstrain is about 0.6 of the theoretical value. This would suggest that, at least as a first approximation, the contribution of overstrain to the total K could be reduced by this 0.6 factor, and a shorter than expected fatigue life would result. This is discussed further in the upcoming comparison of experimental and theoretical results.

No attempt is made to relate the two sets of experimental results in Figure 8, that is the results designated by a dashed line for 50 percent to 100 percent overstrained tubes and the results from the 30 percent and 60 percent overstrained tubes. The reason for this is that the methods used for overstraining were quite different for the two sets of results. A mandrel swaging process was used in the former case and a hydraulic overpressure process was used in the latter case. The different overstraining methods could result in different amounts of Bauschinger effect in the two sets of experimental results.

## LIFE CALCULATIONS

The fatigue growth rate of cracks subjected to cyclic loading may be expressed in terms of Paris' law:<sup>19</sup>

$$\frac{da}{dN} = C(\Delta K)^m \quad (15)$$

where  $da/dN$  is the fatigue crack growth per loading cycle,  $C$  and  $m$  are empirical constants and  $\Delta K$  is the range of stress intensity defined by:

$$\Delta K = K_{\max} - K_{\min} \quad (K_{\min} > 0)$$

$$\Delta K = K_{\max} \quad (K_{\min} < 0)$$

and  $K_{\max}$  and  $K_{\min}$  are respectively the maximum and minimum values of stress intensity during the loading cycle. Note that the possibility of "overlapping" or touching of the crack surfaces at some point on the crack line remote from the crack tip<sup>20</sup> is not considered in this report. During the lifetime of a particular cracked cylinder the crack will propagate from some initial depth  $a_1$  to some final depth  $a_f$ , where  $a_f$  is generally the total wall thickness of the cylinder,  $R_2 - R_1$ . In order to predict the fatigue life, equation (15) is rearranged to give:

$$\int_{a_1}^{a_f} \frac{da}{C(\Delta K)^m} = N_f - N_1 \quad (16)$$

---

<sup>19</sup>Paris, P. C. and Erdogan, F., "A Critical Analysis of Crack Propagation Laws," Trans ASME, J. Bas. Engng., Vol. 85, 1963, pp. 528-534.

<sup>20</sup>Parker, A. P., "Stress Intensity Factors, Crack Profiles, and Fatigue Crack Growth Rates in Residual Stress Fields," presented at ASTM Symposium on Residual Stress Effects in Fatigue, Phoenix, AZ, May 1981.

Crack growth (a versus N) predictions are made for two examples which are near the extremes of crack geometry encountered in thick cylinders, a single nearly straight-fronted crack and a single semi-circular crack. The predictions are compared with ultrasonic crack growth measurements from cylinders in which internal radius  $R_1$  is 90 mm,  $R_2/R_1$  is 2.0, the cyclic pressurization is zero to 331 MPa. The cylinder material is ASTM A723 forged steel, with yield strength of 1175 MPa,  $-40^\circ\text{C}$  Charpy impact energy of 34 J, reduction in area of 50 percent.<sup>21</sup> These properties can be slightly different after overstrain, due to the plastic strain, which can be up to 1 percent at the inner radius of a 100 percent overstrained cylinder. Considering this small amount of plastic strain relative to reduction in area, no significant effect on fatigue life is expected as the result of the material property changes due to the overstrain process.

In general, the integral of Eq. (16) was evaluated numerically using Simpson's rule. For the particular steel employed in the experimental crack growth rate work, the measured constants are:

$$C = 6.52 \times 10^{-12} \quad , \quad m = 3.0$$

for crack growth in meters per cycle and  $\Delta K$  in  $\text{MPa m}^{1/2}$ .

(a) Single, nearly straight-fronted crack

Figure 9 shows a versus N predictions based on the K results presented in Figure 3 for a single, straight-fronted radial crack, initial depth 6.4 mm. The solid lines in Figure 9 are predictions for zero and 30 percent over-

---

<sup>21</sup>Throop, J. F., "Fatigue Crack Growth in Thick-Walled Cylinders," Proceedings of the National Conference on Fluid Power, Fluid Power Society, Chicago, 1972, pp. 115-131.

strain. The dashed line shows experimental results, originally reported in Reference 21, for a tube with zero nominal overstrain in which a single notch was cut using electro-discharge machining to a depth of 6.4 mm and a half surface length,  $c$ , of 254 mm.

For this example it is possible<sup>22</sup> to integrate Eq. (16) directly if a simple, shallow crack  $K$  expression is used, that is, one with  $K_p/K_p$  at a constant value. From Figure 2,  $K_p/K_p = 1.05$  at  $a/R_2 - R_1 = 0.2$  is a reasonable choice, considering that most of the cylinder life is expended at relatively low values of  $a$ . Doing so and combining with Eqs. (6) and (12) gives the following expression for fatigue life of a tube with no overstrain:

$$N_f - N_i = \frac{2 \left[ \frac{1}{\sqrt{a_i}} - \frac{1}{\sqrt{a_f}} \right]}{C \left[ \frac{K_p}{K_p} (\pi)^{1/2} \left( \frac{2R_2^2}{R_2^2 - R_1^2} \right) L_p p \right]^3} \quad (17)$$

For values of  $a_i$ ,  $C$ ,  $R_2$ ,  $R_1$ , and  $p$  in this example and setting  $L_p = 1.0$ , the result is the dotted line in Figure 9, very close to the more general analysis. For the conditions of this comparison, the simpler analysis of Eq. (17), although less rigorous and general, is adequate and easier to use.

The lack of agreement between the two analytical predictions and the experiment would be improved if the shape factor,  $L_p$  was significantly less

<sup>21</sup>Throop, J. F., "Fatigue Crack Growth in Thick-Walled Cylinders," Proceedings of the National Conference on Fluid Power, Fluid Power Society, Chicago, 1972, pp. 115-131.

<sup>22</sup>Underwood, J. H. and Throop, J. F., "Surface Crack  $K$ -Estimates and Fatigue Life Calculations in Cannon Tubes," Part-Through Crack Fatigue Life Prediction, ASTM STP 687, J. B. Chang, Ed., American Society for Testing and Materials, 1979, pp. 195-210.

than unity. The initial shape is described by  $(a/c)_i = 0.025$  and the final shape is  $(a/c)_f = 0.18$ . Referring to Figure 7(a) and considering that most of the cylinder life is expended with low values of both  $a/c$  and  $a/R_2 - R_1$ ,  $L_p$  is estimated to be between 0.95 and 1.0. So even with this factor to the third power in Eq. (17), it cannot account for the differences in Figure 9.

(b) Single, semi-circular crack

Figure 10 shows  $a$  versus  $N$  predictions, based on the  $K$  values presented in Figure 2, as modified in accordance with Eq. (12), utilizing correction factors  $L_p$  and  $L_a$  from Figures 7(a) and 7(c) respectively, for  $a/c = 1.0$ . The  $K$  values are representative of the stress intensity at the deepest point of a semi-circular crack of initial depth 6.4 mm in a thick cylinder, and therefore implicitly assume that the crack retains its semi-circular shape during the life of the tube. This assumption appears to be justified on the basis of experimental observations.<sup>16</sup> The predictions are made for zero, 30 percent, 40 percent, 45 percent, and 50 percent overstrain, while the dashed lines indicate experimental results<sup>16</sup> for the same initial crack depth for actual tubes with zero, 30 percent, and 60 percent nominal overstrain.

For this example it is also possible to obtain a closed form expression for fatigue life, analogous to Eq. (17). By combining Eqs. (6), (8), and (10) it can be shown that the ratio of the  $K$  expression for an autofrettaged and pressurized cylinder to that of a pressurized cylinder with no autofrettage is the following:

---

<sup>16</sup>Underwood, J. H. and Throop, J. F., "Residual Stress Effects on Fatigue Cracking of Pressurized Cylinders and Notched Bending Specimens," presented at Fourth SESA International Congress, Boston, MA, May 1980

$$\frac{K_{p+A}}{K_p} = 1 + \frac{Y}{p} \left[ \ln \left( \frac{R_2}{R_A} \right) + \delta \ln \frac{R_1}{R_2} + \frac{R_A^2 - \delta R_1^2 - (1-\delta)R_2^2}{2R_2^2} \right] \quad (18)$$

where  $\delta$  is defined as  $\frac{K_A/K_A}{K_p/K_p}$ , the ratio of the K solutions in Figure 2.

Using Eq. (18) in a life expression in the form of Eq. (17) gives  $N_f - N_i =$

$$\frac{2 \left[ \frac{1}{\sqrt{a_1}} - \frac{1}{\sqrt{a_f}} \right]}{C \left[ \frac{K_p}{K_p} (\pi)^{1/2} \left( \frac{2R_2^2}{R_2^2 - R_1^2} \right) \left( 1 + \frac{Y}{p} \left[ \ln \left( \frac{R_2}{R_A} \right) + \delta \ln \frac{R_1}{R_2} + \frac{R_A^2 - \delta R_1^2 - (1-\delta)R_2^2}{2R_2^2} \right] \right) L_p \right]^3} \quad (19)$$

which should give a good estimate of fatigue life for an autofrettaged, pressurized cylinder in which a shallow semi-elliptical crack dominates the life. Results from this shallow crack expression are shown in Figure 10 for 0 percent, 30 percent, and 50 percent overstrain. A mean  $\bar{L} = 0.53$  was used, since  $L_p$  and  $L_A$  are close to this value for  $a/R_2 - R_1 = 0.2$ , see Figures 7(a) and 7(c). The predictions of the shallow crack analysis, Eq. (19), are close to those of the more general analysis. The lack of agreement between the two analytical predictions and the experiments is discussed in the upcoming section.

#### DISCUSSION AND CONCLUSIONS

Life prediction for cracked tubes requires an accurate knowledge of stress intensity factor at short crack depths. In this report two-dimensional solutions for cracked tubes with various amounts of residual stress (overstrain) were obtained by use of the modified mapping collocation technique,

which gives good convergence to the known analytic solution at very small crack depths.

The solutions were extended to include three-dimensional semi-elliptical cracks in thick cylinders by calculating the proportion of tension and bending in the cylinder and applying appropriate correction factors determined for cracked plates in tension and bending. Comparison with limited available three dimensional solutions for thick cylinders indicates good agreement at short to medium crack lengths,  $a/c \leq 0.3$ , wherein most of the fatigue lifetime is expended. The approach adopted is however, not restricted to thick cylinders, and may have some application in Fracture Mechanics Design. Indeed, the thick cylinder may be a sort of limiting configuration in which maximum errors would be anticipated because of the large degree of restraint offered by the doubly connected body.

The calculations of life for non-autofrettagged, pressurized tubes with nearly straight-fronted and semi-circular cracks predict lives of about one quarter of those determined experimentally. Possible explanations for this effect are:

- a. The possibility that full pressure does not infiltrate the crack. This is not considered likely since the experimental work was deliberately designed to avoid this effect. It could be far more noticeable in the autofrettage case if it were so, because of the compressive stress closing the crack.
- b. Residual stresses in the non-autofrettage tube. Again, this is not considered likely. When tested, non-autofrettagged tubes do not exhibit any tendency to spring open, indicating negligible gross residual stresses.

c. Multiple, small, semi-elliptical cracks along the notch boundary. This is considered a probable explanation. Such a form of multiple crack growth would result in slower overall crack growth than that of a single crack, until the individual semi-elliptical cracks linked to form a single continuous crack front.

Lifetimes calculated on the basis of the 'ideal' residual stress field indicate extreme sensitivity to the amount of overstrain. Note in Figure 10 that an increase from 30 to 50 percent overstrain increases the predicted life by a factor of five, while an increase from 30 to 60 percent overstrain increases measured life by a factor of 1.4. So there is clearly much less increase in life due to increased overstrain than would be expected from the calculations. We believe this effect is directly related to the less than expected opening angle measured from cylinders with 60 percent overstrain, discussed in relation to Figure 8. The preferred explanation for the deviations of opening angle and lifetime from calculated values is the reduction in the residual stress field due to reversed yielding near the inner radius caused by the Bauschinger effect. This would manifest itself as a reduction in opening angle, particularly at large overstrains, and a relatively larger reduction in lifetime, since most of the lifetime is expended at shallow depths at which the hoop stresses are reduced most significantly.

#### REFERENCES

1. Tan, C. L. and Fenner, R. T., "Stress Intensity Factors for Semi-Elliptical Surface Cracks in Pressurized Cylinders Using the Boundary Integral Equation Method," Int. J. Fracture, Vol. 16, No. 3, 1980, pp. 233-246.
2. Andriano, G. P. and Parker, A. P., "Weight Functions for Cracked Curved Beams," in Numerical Methods in Fracture Mechanics, D. R. J. Owen and A. K. Chakrabarti (eds.), Proceedings Second International Conference, Swansea, 1981, pp. 17-22.
3. Muskhelishvili, G. I., Some Basic Problems of the Mathematical Theory of Elasticity, Noordhoff, 1973.
4. Tracey, P. G., "Elastic Analysis of Radial Cracks Emanating From the Outer and Inner Surfaces of a Circular Ring," Engng. Frac. Mech., Vol. 11, 1979, pp. 391-400.
5. Eason, E. D., "A Review of Least Squares Methods for Solving Partial Differential Equations," Int. J. Num. Meth. in Engng., Vol. 10, 1976, pp. 1021-1046.
6. Sih, G. C., Paris, P. C., and Erdogan, F., "Crack Tip Stress Intensity Factors for Cracks in Plates Under Extension and Plate Bending Problems," J. Appl. Mech., Vol. 30, 1963, pp. 305-311.
7. Tracey, P. G. and Freese, C. E., "Elastic Analysis For a Radial Crack in a Circular Ring," Engineering Fracture Mechanics, Vol. 4, No. 2, 1972, pp. 315-321.

8. Grandt, A. F., "Stress Intensity Factors for Cracked Holes and Rings Loaded With Polynomial Crack Face Pressure Distributions," Int. J. Fracture, Vol. 14, 1978, pp. R221-R229.
9. Hill, R., The Mathematical Theory of Plasticity, Clarendon Press, Oxford, 1950.
10. Grandt, A. F., "Two Dimensional Stress Intensity Factor Solutions For Radially Cracked Rings," AFML-TR-75-121, Air Force Materials Lab, Wright Patterson AFB, Ohio, 1975.
11. Parker, A. P. and Farrow, J. R., "Stress Intensity Factors for Multiple Radial Cracks Emanating From the Bore of an Autofrettaged or Thermally Stressed Thick Cylinder," Engng. Frac. Mech., Vol. 14, 1981, pp. 237-241.
12. Parker, A. P., "Stress Intensity and Fatigue Crack Growth in Multiply-Cracked, Pressurized, Partially Autofrettaged Thick Cylinders," Fatigue of Engng. Materials and Structures (in press).
13. Newman, J. C. and Raju, I. S., "Analyses of Surface Cracks in Finite Plates Under Tension or Bending Loads," NASA TP 1578, 1979.
14. Atulri, N. and Kathiresan, K., "3D Analyses of Surface Flaws in Thick-Walled Reactor Pressure-Vessels Using Displacement-Hybrid Finite Element Method," Nuclear Engng. and Design, Vol. 51, 1979, pp. 163-176.
15. Rooke, D. P. and Cartwright, D. J., Compendium of Stress Intensity Factors, Her Majesty's Stationery Office, London, 1976.
16. Underwood, J. H. and Throop, J. F., "Residual Stress Effects on Fatigue Cracking of Pressurized Cylinders and Notched Bending Specimens," presented at Fourth SESA International Congress, Boston, MA, May 1980.

17. Milligan, R. V., Koo, W. H., Davidson, T. E., "The Bauschinger Effect in a High-Strength Steel," Trans. ASME, J. Bas. Engineering, Vol. 88, 1966, pp. 480-488.
18. Parker, A. P. and Farrow, J. R., "On the Equivalence of Axisymmetric Bending, Thermal, and Autofrettage Residual Stress Fields," J. Strain Analysis, Vol. 15, No. 1, 1980, pp. 51-52.
19. Paris, P. C. and Erdogan, F., "A Critical Analysis of Crack Propagation Laws," Trans ASME, J. Bas. Engng., Vol. 85, 1963, pp. 528-534.
20. Parker, A. P., "Stress Intensity Factors, Crack Profiles, and Fatigue Crack Growth Rates in Residual Stress Fields," presented at ASTM Symposium on Residual Stress Effects in Fatigue, Phoenix, Arizona, May 1981.
21. Throop, J. F., "Fatigue Crack Growth in Thick-Walled Cylinders," Proceedings of the National Conference on Fluid Power, Fluid Power Society, Chicago, 1972, pp. 115-'31.
22. Underwood, J. H. and Throop, J. F., "Surface Crack K-Estimates and Fatigue Life Calculations in Cannon Tubes," Part-Through Crack Fatigue Life Prediction, ASTM STP 687, J. B. Chang, Ed., American Society for Testing and Materials, 1979, pp. 195-210.

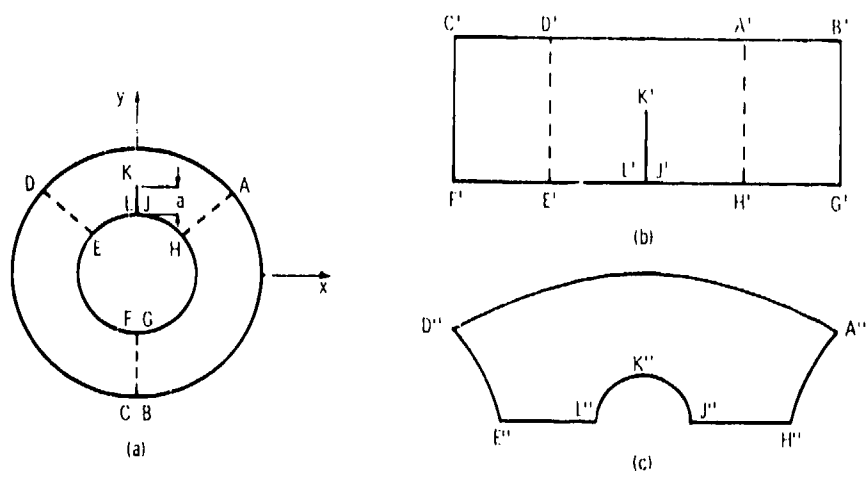


Figure 1. Cracked thick cylinder geometry showing partitioning and mapping scheme (a)  $z$  (physical plane), (b)  $\xi$  plane, (c)  $\zeta$  plane.

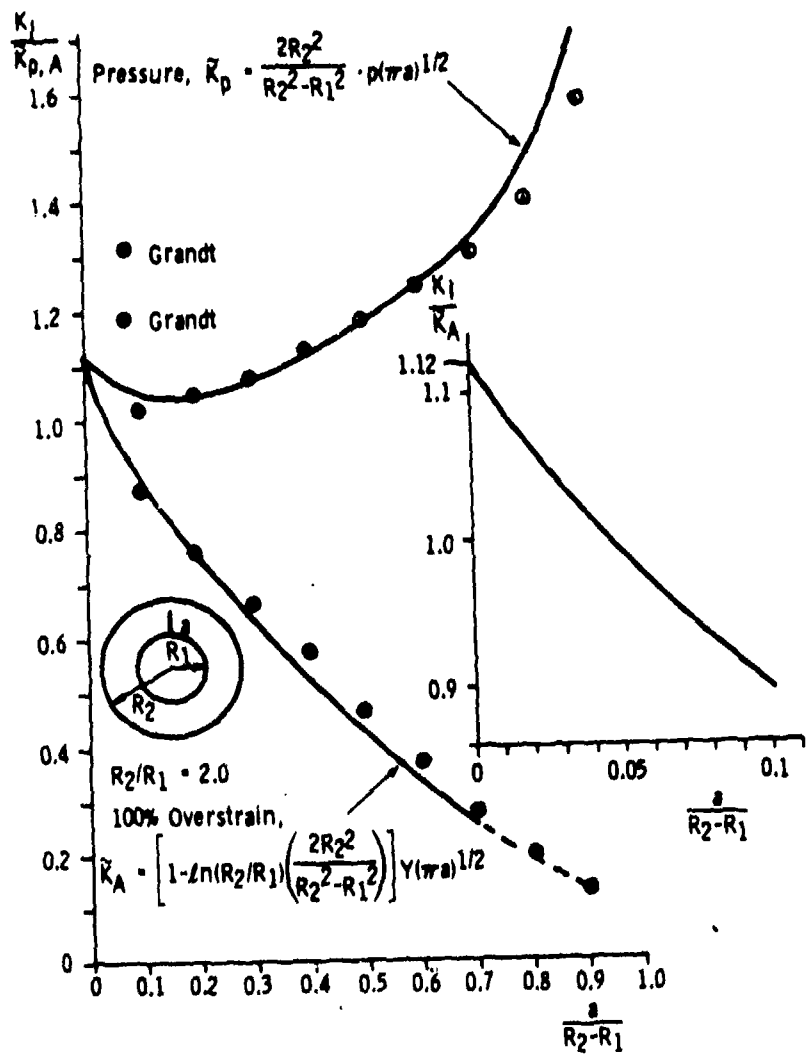


Figure 2. Stress intensity factors for a single, straight-fronted, radial crack in a thick cylinder. (Inset) Short crack length convergence for 100 percent overstrain.

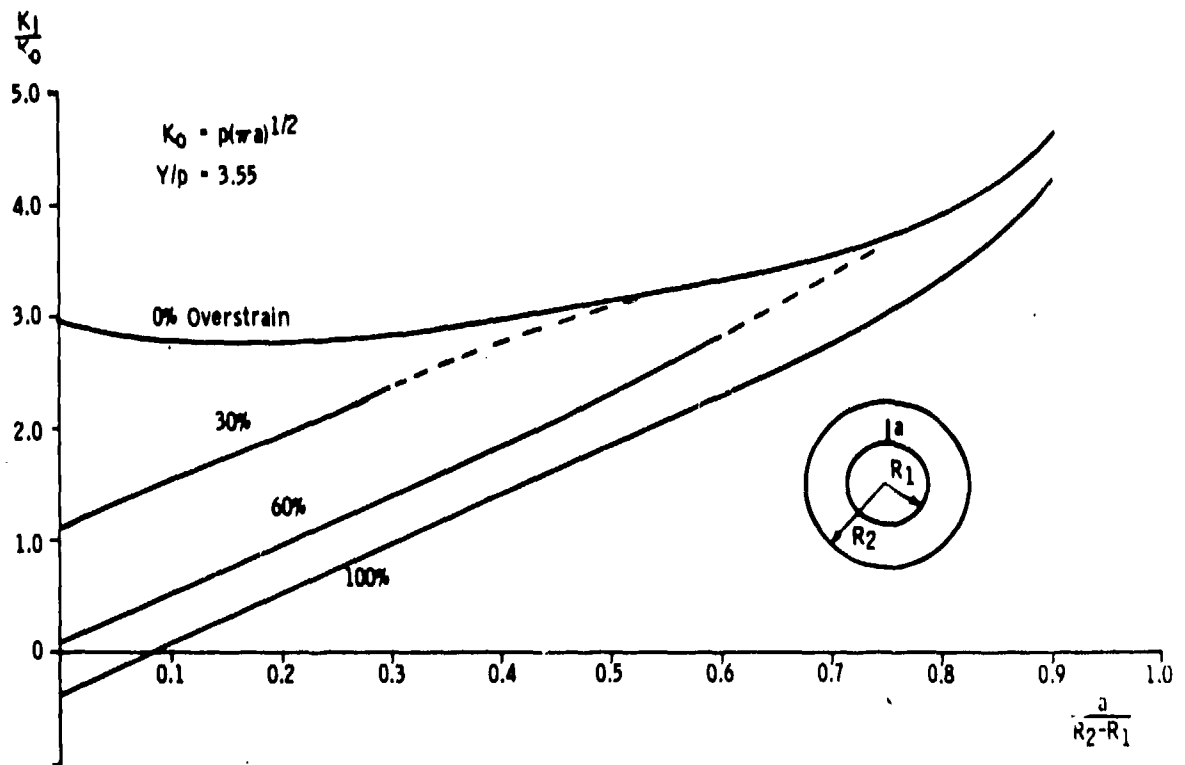


Figure 3. Stress intensity factors for a single, straight-fronted crack in a pressurized thick cylinder with 0 percent, 30 percent, 60 percent, and 100 percent overstrain.

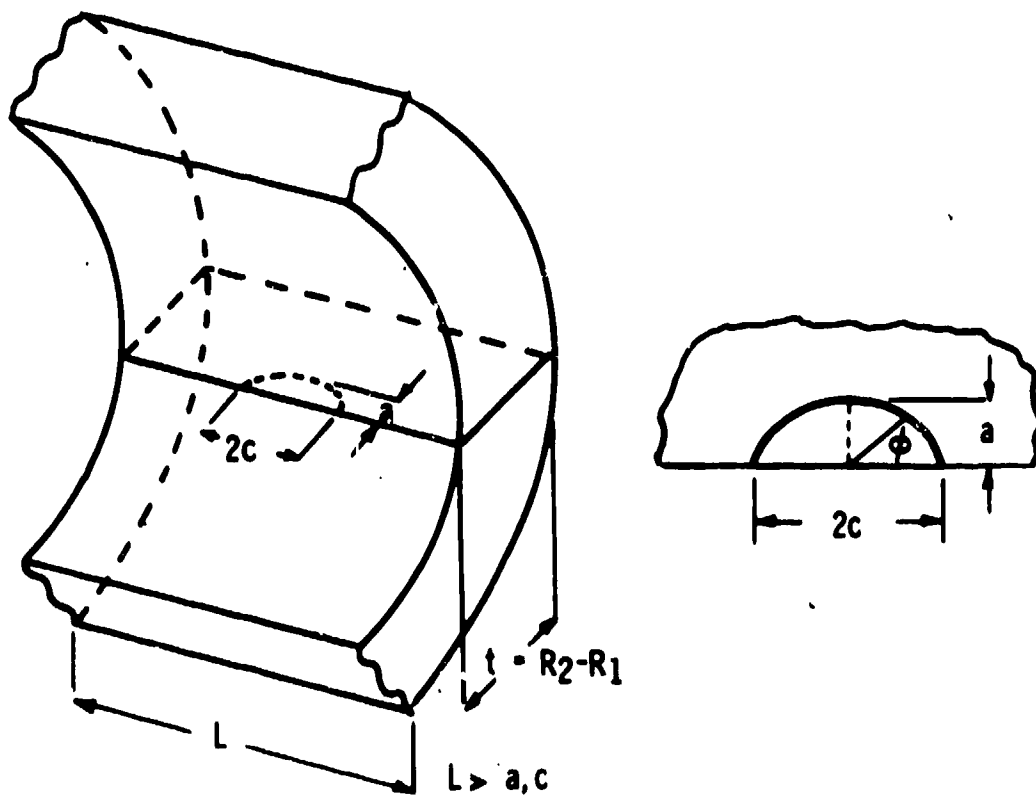


Figure 4. Semi-elliptical crack in a thick cylinder.

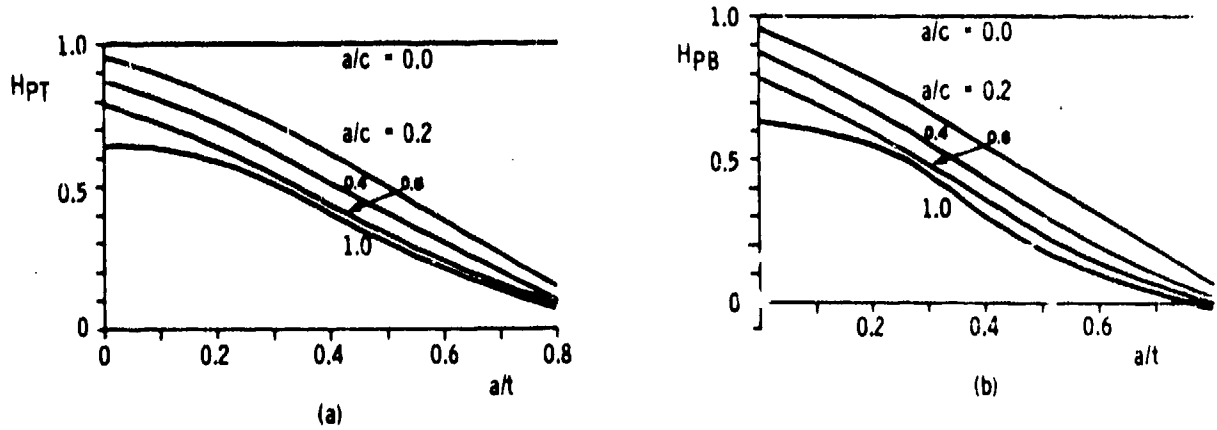


Figure 5. (a) Crack shape factors for a plate in tension ( $\phi = \pi/2$ ), after Reference 13.  
 (b) Crack shape factors for a plate in pure bending ( $\phi = \pi/2$ ), after Reference 13.

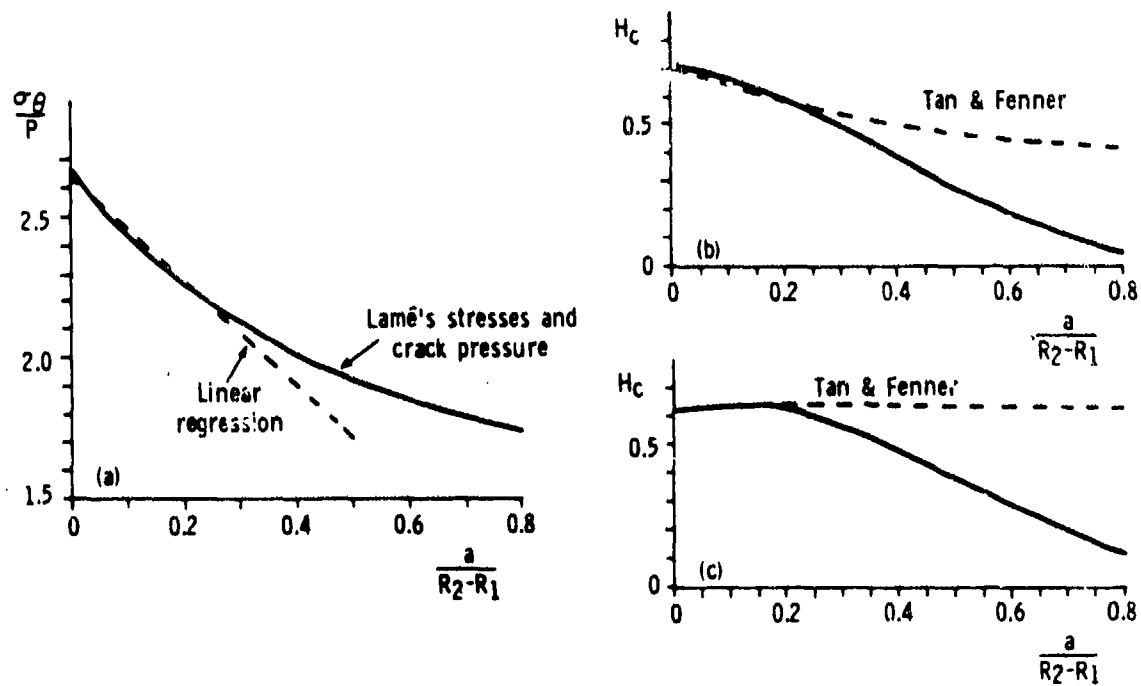


Figure 6. (a) Method of calculating proportion of tension and bending, pressure in bore and cracks.  
 (b) Crack shape factors for pressure in bore and cracks,  $a/c = 0.8$ ,  $\phi = \pi/2$ .  
 (c) Crack shape factors for pressure in bore and cracks,  $a/c = 0.8$ ,  $\phi = 0$ .

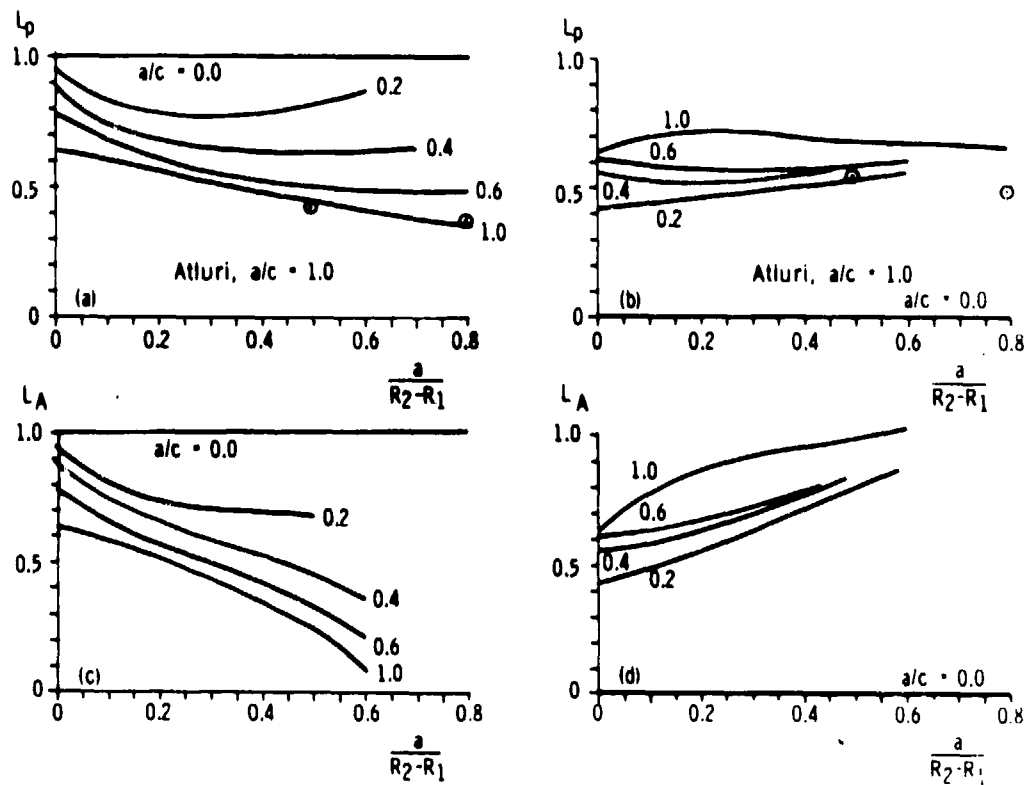


Figure 7. (a) Crack shape factors,  $L_p$ , for pressure in bore and cracks,  $\phi = \pi/2$ ; two data points from Reference 14,  $a/c = 1.0$ .  
 (b) Crack shape factors,  $L_p$ , for pressure in bore and cracks,  $\phi = 0$ ; two data points from Reference 14,  $a/c = 1.0$ .  
 (c) Crack shape factors,  $L_A$ , for 100 percent overstrain,  $\phi = \pi/2$ .  
 (d) Crack shape factors,  $L_A$ , for 100 percent overstrain,  $\phi = 0$ .

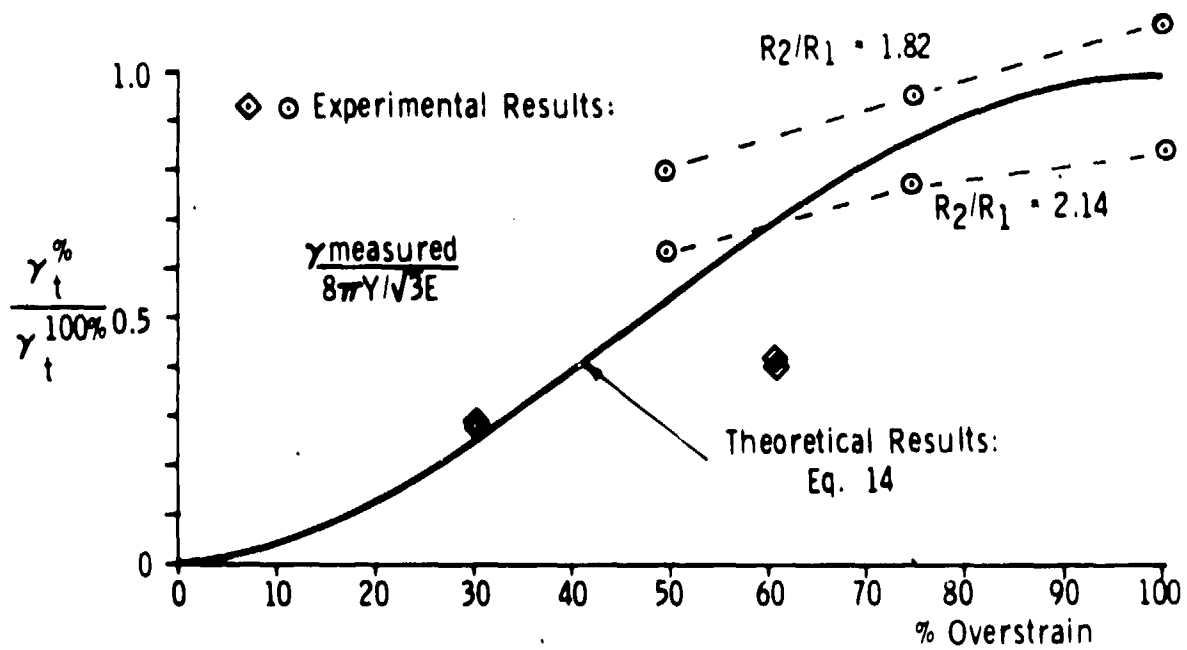


Figure 8. Ratio of opening angle for partial overstrain to the theoretical value for 100 percent overstrain.

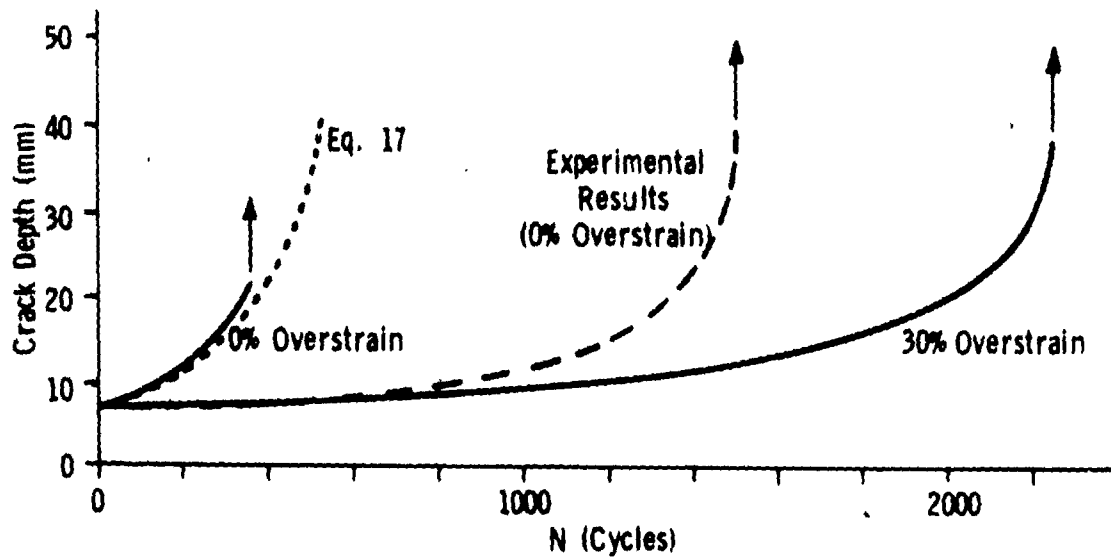


Figure 9. Fatigue crack growth ( $a$  versus  $N$ ) in thick cylinder with single, straight-fronted crack; experimental results and predictions.

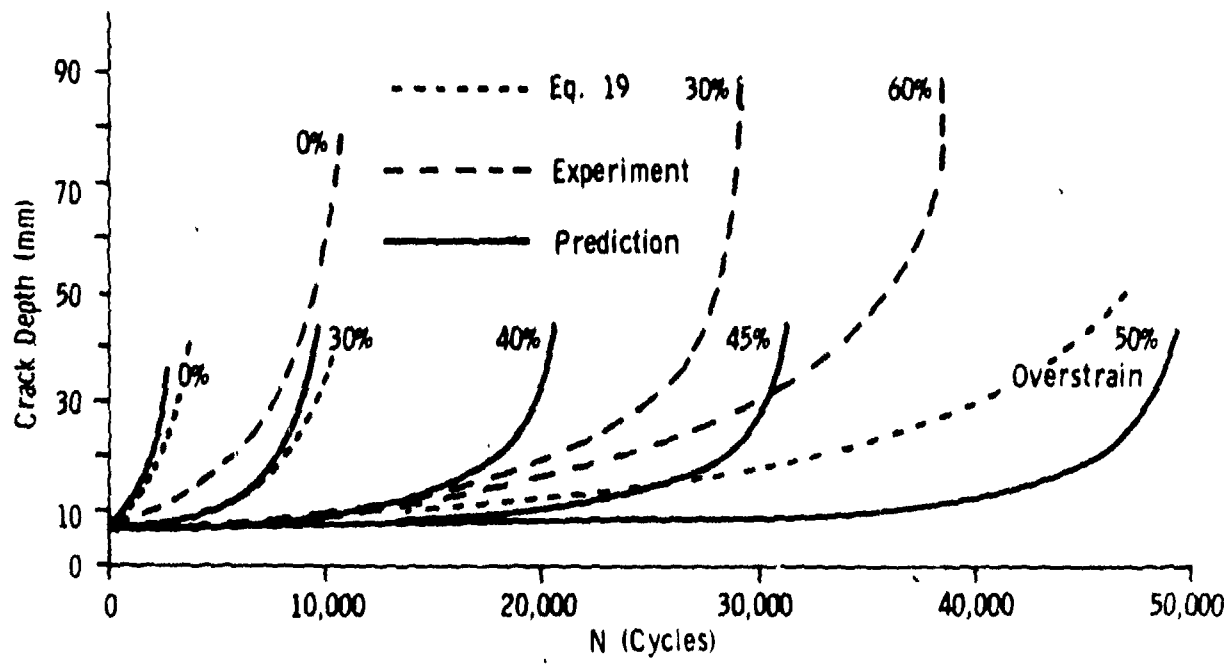


Figure 10. Fatigue crack growth (a versus N) in thick cylinder with single, semi-circular crack; experimental results and predictions.

## APPENDIX

### OPENING OF CUT TUBES WITH PARTIAL AUTOFRETTAGE - NO REVERSED YIELDING

The residual stresses in an autofrettaged tube, internal radius  $R_1$ , external radius  $R_2$ , autofrettage radius  $R_A$  are:<sup>A1</sup>

$$\sigma_{\theta 1} = -p + Y(1 + \ln(r/R_1)) - p \left( \frac{R^2}{R_2^2 - R_1^2} \left[ 1 + \frac{R_2^2}{r^2} \right] \right), \quad R_1 < r < R_A \quad (A1)$$

$$\sigma_{\theta 2} = \left[ \frac{Y R_A^2}{2 R_2^2} - \frac{p R_1^2}{R_2^2 - R_1^2} \right] \left[ 1 + \frac{R_2^2}{r^2} \right], \quad R_A < r < R_2 \quad (A2)$$

where  $p$ , the autofrettage pressure is given by:

$$p = Y \ln(R_A/R_1) + \frac{Y}{2 R_2^2} (R_2^2 - R_A^2) \quad (A3)$$

The total moment acting over any radial cut is given by:

$$M = \int_{R_1}^{R_2} \sigma_{\theta} \cdot r \cdot dr$$

or

$$M = \int_{R_1}^{R_A} \sigma_{\theta 1} r \cdot dr + \int_{R_A}^{R_2} \sigma_{\theta 2} r \cdot dr \quad (A4)$$

Since the opening angle of fully autofrettaged tubes of any radius ratio,  $R_2/R_1$ , provided reversed yielding does not occur, is given by  $8\pi Y/\sqrt{3}E$ ,<sup>A2</sup> and the amount of opening is proportional to the applied bending moment, it is

<sup>A1</sup>Hill, R., The Mathematical Theory of Plasticity, Clarendon Press, Oxford, 1950.

<sup>A2</sup>Parker, A. P. and Farrow, J. R., "On the Equivalence of Axisymmetric Bending, Thermal, and Autofrettage Residual Stress Fields," J. Strain Analysis, Vol. 15, No. 1, 1980, pp. 51-52.

possible to produce a non-dimensionalized plot of theoretical angle of opening for a cut tube with partial autofrettage, for any radius ratio. The curve for  $R_2/R_1 = 2.0$  is shown in Figure 8 of the main report. Deviations from this curve for  $1.8 < R_2/R_1 < 2.2$  are less than 1 percent of the maximum opening.

#### OPENING OF CUT TUBES WITH PARTIAL AUTOFRETTAGE - WITH REVERSED YIELDING

If the material of the tube has a reduced yield strength in compression of  $-\lambda Y$ , it may undergo reversed yielding out to a radius  $R_D$  after removal of the autofrettage pressure,  $p$ . In this case the residual stresses are:<sup>A3</sup>

$$\sigma_{\theta 3} = -\lambda Y (1 + \ln(r/R_1)) \quad , \quad R_1 < r < R_D \quad (A5)$$

$$\sigma_{\theta 4} = -\left\{ p - (1+\lambda) Y \ln \left( \frac{R_D}{R_1} \right) \right\} \frac{R_D^2}{R_2^2 - R_D^2} \left[ 1 + \frac{R_2^2}{r^2} \right]$$

$$-p + Y (1 + \ln(r/R_1)) \quad , \quad R_D < r < R_A \quad (A6)$$

$$\sigma_{\theta 5} = \left[ \frac{Y R_A^2}{2 R_2^2} - \left\{ p - (1+\lambda) Y \ln \left( \frac{R_D}{R_1} \right) \right\} \frac{R_D^2}{R_2^2 - R_D^2} \right] \left[ 1 + \frac{R_2^2}{r^2} \right] \quad , \quad R_A < r < R_2 \quad (A7)$$

where  $R_D$  is calculated in an iterative fashion from:

$$\frac{p}{Y} = (1+\lambda) \left[ \frac{R_2^2 - R_D^2}{2 R_2^2} + \ln(R_D/R_1) \right] \quad (A8)$$

Once again, the total moment acting over any radial cut is given by equation (A4), thus when reversed yielding occurs:

$$M = \int_{R_1}^{R_D} \sigma_{\theta 3} r \cdot dr + \int_{R_D}^{R_A} \sigma_{\theta 4} r \cdot dr + \int_{R_A}^{R_2} \sigma_{\theta 5} r \cdot dr \quad (A9)$$

<sup>A3</sup>Parker, A. P., Sleeper, K. A., and Andrasic, C. P., "Safe Life Design of Gun Tubes, Some Numerical Methods and Results," US Army Numerical Analysis and Computers Conference, Huntsville, AL (1981) (in press).

The reduction in opening arising from a Bauschinger effect equivalent to  $\lambda = 0.5$  can be calculated, leading to a plot similar to Figure 8 of the main report. The maximum reduction in opening is approximately 8 percent as a result of this magnitude of Bauschinger effect. Deviations from this figure do not exceed 1 percent for  $1.8 < R_2/R_1 < 2.2$ .

#### APPENDIX REFERENCES

- A1. Hill, R., The Mathematical Theory of Plasticity, Clarendon Press, Oxford, 1950.
- A2. Parker, A. P. and Farrow, J. R., "On the Equivalence of Axisymmetric Bending, Thermal, and Autofrettage Residual Stress Fields," J. Strain Analysis, Vol. 15, No. 1, 1980, pp. 51-52.
- A3. Parker, A. P., Sleeper, K. A., and Andrasic, C. P., "Safe Life Design of Gun Tubes, Some Numerical Methods and Results," US Army Numerical Analysis and Computers Conference, Huntsville, AL (1981) (in press).

TECHNICAL REPORT INTERNAL DISTRIBUTION LIST

	<u>NO. OF COPIES</u>
CHIEF, DEVELOPMENT ENGINEERING BRANCH	1
ATTN: DRDAR-LCB-DP	1
-DR	1
-DS (SYSTEMS)	1
-DS (ICAS GROUP)	1
-DC	1
CHIEF, ENGINEERING SUPPORT BRANCH	1
ATTN: DRDAR-LCB-SE	1
CHIEF, RESEARCH BRANCH	2
ATTN: DRDAR-LCB-R (ELLEN FOGARTY)	1
-RA	1
-RM	1
-RP	1
-RT	1
TECHNICAL LIBRARY	5
ATTN: DRDAR-LCB-TL	
TECHNICAL PUBLICATIONS & EDITING UNIT	2
ATTN: DRDAR-LCB-TL	
DIRECTOR, OPERATIONS DIRECTORATE	1
DIRECTOR, PROCUREMENT DIRECTORATE	1
DIRECTOR, PRODUCT ASSURANCE DIRECTORATE	1

NOTE: PLEASE NOTIFY DIRECTOR, BENET WEAPONS LABORATORY, ATTN: DRDAR-LCB-TL,  
OF ANY REQUIRED CHANGES.

TECHNICAL REPORT EXTERNAL DISTRIBUTION LIST

	<u>NO. OF COPIES</u>		<u>NO. OF COPIES</u>
ASST SEC OF THE ARMY RESEARCH & DEVELOPMENT ATTN: DEP FOR SCI & TECH THE PENTAGON WASHINGTON, D.C. 20315	1	COMMANDER ROCK ISLAND ARSENAL ATTN: SARRI-ENM (MAT SCI DIV) ROCK ISLAND, IL 61299	1
COMMANDER DEFENSE TECHNICAL INFO CENTER ATTN: DTIC-DDA CAMERON STATION ALEXANDRIA, VA 22314	12	DIRECTOR US ARMY INDUSTRIAL BASE ENG ACT ATTN: DRXIB-M ROCK ISLAND, IL 61299	1
COMMANDER US ARMY MAT DEV & READ COMD ATTN: DRCDE-SG 5001 EISENHOWER AVE ALEXANDRIA, VA 22333	1	COMMANDER US ARMY TANK-AUTMV R&D COMD ATTN: TECH LIB - DRSTA-TSL WARREN, MICHIGAN 48090	1
COMMANDER US ARMY ARRADCOM. ATTN: DRDAR-LC DRDAR-LCA (PLASTICS TECH EVAL CEN)	1	COMMANDER US ARMY TANK-AUTMV COMD ATTN: DRSTA-RC WARREN, MICHIGAN 48090	1
DRDAR-LCE	1	COMMANDER US MILITARY ACADEMY ATTN: CHMN, MECH ENGR DEPT WEST POINT, NY 10996	1
DRDAR-LCM (BLDG 321)	1		
DRDAR-LCS	1	US ARMY MISSILE COMD REDSTONE SCIENTIFIC INFO CEN	
DRDAR-LCU	1	ATTN: DOCUMENTS SECT, BLDG 4484	2
DRDAR-LCW	1	REDSTONE ARSENAL, AL 35898	
DRDAR-TSS (STINFO)	2		
DOVER, NJ 07801		COMMANDER US ARMY FGN SCIENCE & TECH CEN ATTN: DRXST-SD 220 7TH STREET, N.E. CHARLOTTESVILLE, VA 22901	1
DIRECTOR US ARMY BALLISTIC RESEARCH LABORATORY ATTN: DRDAR-TSB-S (STINFO) ABERDEEN PROVING GROUND, MD 21005	1	COMMANDER US ARMY MATERIALS & MECHANICS RESEARCH CENTER ATTN: TECH LIB - DRXMR-PL WATERTOWN, MASS 02172	2
COMMANDER US ARMY ARRCOM ATTN: DRSAR-LEP-L ROCK ISLAND ARSENAL ROCK ISLAND, IL 61299	1		

NOTE: PLEASE NOTIFY COMMANDER, ARRADCOM, ATTN: BENET WEAPONS LABORATORY, DRDAR-LCB-TL, WATERVLIET ARSENAL, WATERVLIET, N.Y. 12189, OF ANY REQUIRED CHANGES.

TECHNICAL REPORT EXTERNAL DISTRIBUTION LIST (CONT.)

	<u>NO. OF COPIES</u>		<u>NO. OF COPIES</u>
COMMANDER US ARMY RESEARCH OFFICE ATTN: CHIEF, IPO P.O. BOX 12211 RESEARCH TRIANGLE PARK, NC 27709	1	DIRECTOR US NAVAL RESEARCH LAB ATTN: DIR, MECH DIV CODE 26-27 (DOC LIB) WASHINGTON, D.C. 20375	1 1
COMMANDER US ARMY HARRY DIAMOND LAB ATTN: TECH LIB 2800 POWDER MILL ROAD ADELPHIA, MD 20783	1	METALS & CERAMICS INFO CEN BATTELLE COLUMBUS LAB 505 KING AVE COLUMBUS, OHIO 43201	1
COMMANDER NAVAL SURFACE WEAPONS CEN ATTN: TECHNICAL LIBRARY CODE X212 DAHLGREN, VA 22448	1	MATERIEL SYSTEMS ANALYSIS ACTV ATTN: DRSXY-MP ABERDEEN PROVING GROUND MARYLAND 21005	1

NOTE: PLEASE NOTIFY COMMANDER, ARRADCOM, ATTN: BENET WEAPONS LABORATORY,  
DRDAR-LCB-TL, WATERVLIET ARSENAL, WATERVLIET, N.Y. 12189, OF ANY  
REQUIRED CHANGES.